The 9th of International Symposium on Transport Phenomena and Dynamics of Rotating Machinery
Honolulu, Hawaii, February 10-14, 2002

THREE-DIMENSIONAL ANALYSIS OF ROTORDYNAMIC FLUID FORCES ON WHIRLING AND CAVITATING FINITE-LENGTH INDUCERS

Luca d'Agostino
Professor,
Dipartimento di Ingegneria Aerospaziale, Università di Pisa,
5 Via G. Caruso, 56126 Pisa, Italy;
Luca.dagostino@ing.unipi.it

Marco R. Venturini Autieri*
M.S. Student,
Dipartimento di Ingegneria Aerospaziale, Università di Pisa,
18033911@studenti.unipi.it

ABSTRACT

The paper investigates the linearized dynamics of the three-dimensional flow in finite-length helical inducers with attached blade cavitation, with the purpose of understanding the impact of the cavitating flow response on the rotordynamic forces exerted by the fluid on the impeller of whirling turbopumps. The flow in the inducer annulus is modeled as a fully-guided, incompressible and inviscid liquid. Cavitation is included through the boundary conditions on the suction sides of the blades, where it is assumed to occur uniformly in a small layer of given thickness. The complex acoustic admittance of the cavitating layer depends on the void fraction of the vapor phase and the parametric value of the phase-shift damping used to account for the energy dissipation. Constant boundary conditions for the total pressure are imposed at the inlet and outlet sections of the inducer blade channels. The three-dimensional unsteady governing equations are written in rotating "body fitted" orthogonal helical coordinates, linearized for small-amplitude whirl perturbations of the mean steady flow, and solved by modal decomposition. The whirl excitation and the boundary conditions generate internal flow resonances in the blade channels of the inducer, leading to a complex dependence of the lateral rotordynamic fluid forces on the whirl speed, the properties of the cavitating layer and the flow coefficient of the machine. Multiple subsynchronous and supersynchronous resonances are predicted. At higher levels of cavitation the amplitudes of the resonances decrease and their frequencies approach the rotational speed (synchronous conditions). Comparison with available experimental data indicates that the present theory correctly evaluates the observed magnitude of the rotordynamic forces as functions of the whirl frequency and their stabilizing or destabilizing effects on the whirl motion. The results may help in understanding the origin and sustain of some of the most critical and destructive instabilities in whirling and cavitating turbopumps.

INTRODUCTION

It is widely recognized that turbopump cavitation can promote the onset of dangerous self-sustained whirl instabilities (Rosenmann, 1965) and substantially alters the behavior of fluid-induced rotordynamic forces on helical inducers (Arndt and Franz, 1986; Brennen, 1994; Bhattacharyya, 1994). Previous research efforts have mainly focused on the origin and analysis of rotordynamic impeller forces for noncavitating conditions (Chamieh et al., 1985; Jery et al., 1985; Jery, 1987; Shoji and Ohasi, 1987; Ohasi and Shoji, 1987; Adkins and Brennen, 1988; Tsujimoto et al., 1997; Uy and Brennen, 1999; Baskharone, 1999). Because of their greater complexity, rotordynamic fluid forces in whirling and cavitating turbopump inducers have so far received comparatively less attention in the open literature and a satisfactory understanding of their behavior is still lacking. The available experimental evidence indicates that cavitation reduces the magnitude of the rotordynamic fluid forces, significantly affecting the added mass of the rotor. It is worth noting that the consequent increase of the critical speeds is of special relevance to highly-loaded supercritical machines, as commonly used in liquid propellant rocket feed systems. A second major effect of cavitation is the introduction of a complex oscillatory dependence of the rotordynamic fluid forces on the whirl frequency. This finding seems to indicate the possible

*Contacting author

occurrence of resonance phenomena in the compressible cavitating flow inside the blade channels under the excitation imposed by the eccentric motion of the rotor. Earlier theoretical analyses have addressed the case of infinitely-long whirling helical inducers with uniformly distributed travelling bubble cavitation (d'Auria et al., 1995; d'Agostino and d'Auria, 1997; d'Agostino et al., 1998). The results confirmed the presence of internal flow resonances and indicate that bubble dynamic effects do not play a major role, except, perhaps, at extremely high whirl speeds. They also suggest that the assumptions of uniformly-distributed bubbly cavitation and infinitely long inducers may contribute to explain the discrepancies between theoretical predictions and experimental data. Following up on this work, we now investigate the dynamics of the unsteady three-dimensional flow in finite-length helical inducers with attached blade cavitation. Upon introduction of suitable simplifying approximations, the flow is linearized for small-amplitude whirl motions of the rotor and solved by modal expansion. In spite of the simplifications introduced in order to obtain an efficient closed form solution, comparison with the available experimental data indicates that the present analysis correctly predicts some of the observed features of the rotordynamic fluid forces in cavitating inducers and provides useful practical indications and fundamental understanding of their dependence on the relevant flow conditions and parameters.

NOMENCLATURE

a	sound speed
A	cross-sectional flow area
b	boundary equation
c	specific heats, constant
$\boldsymbol{e}$	unit vector
f	nondimensional force
F	force
$\imath$	imaginary unit
I	modified Bessel function of the first kind, integral
j	blade index
J	Bessel function of the first kind
k	hub excitation mode index
K	modified Bessel function of the second kind
K_C	cavitating layer parameter
L	axial length of the inducer
L^*	blade axial length
l	blade excitation mode index
m	streamwise mode index
n	blade-to-blade helical coordinate
N	blade-to-blade mode function
N_B	number of blades
N_R	number of blade revolutions
$O,\, O^*$	origin of coordinate systems
p	pressure
p_t	total or stagnation pressure
P	blade axial pitch
P^*	blade-to-blade distance
$\dot{Q}$	volume flow rate
r	radial coordinate, radius
$\boldsymbol{r}$	radial vector
R	radial mode function, cavity radius
s	streamwise helical coordinate
S	surface, streamwise mode function
t	time
T	temperature
u	radial velocity component
$\boldsymbol{u}$	velocity vector
v	azimuthal velocity component
w	axial velocity component
x	abscissa
y	ordinate
Y	Bessel function of the second kind
z	axial coordinate
α	void fraction
β	blade angle
δ	cavitation layer thickness
δ_T	thermal boundary layer thickness
ε	whirl eccentricity
ζ	nondimensional damping coefficient
ϑ	azimuthal angle
λ	radial eigenvalue
μ	streamwise eigenvalue
ν	blade-to-blade eigenvalue
ρ	density
σ	cavitation number
φ	velocity potential
ϕ	flow coefficient
ω	whirl angular velocity
Ω	inducer rotational speed

Subscripts and Superscripts

B	blade
C	cavitation
F	mean flow
H	hub
L	liquid
M	mean
R	radial
T	tangential, blade tip
V	vapor
$\overline{q}$	unperturbed value of q
$\tilde{q}$	perturbation value of q
$\hat{q}$	complex representation of $\tilde{q}$
q'	derivative, value of q in the rotating frame
q^*	value of q in the inducer-fixed frame
1	inducer inlet
2	inducer outlet

LINEARIZED DYNAMICS OF THE CAVITATING FLOW IN A WHIRLING INDUCER

We examine the dynamics of an incompressible, inviscid liquid of velocity $\boldsymbol{u}$, pressure p, and density ρ_L in a helical inducer rotating with velocity Ω and whirling on a circular orbit of small eccentricity ε at angular speed ω. A number of simplifications are introduced in order to reduce the problem to a form admitting an analytical solution. As illustrated in Figure 1, a simple helical inducer is considered, with N_B radial blades, zero blade thickness, axial length L, hub radius r_H, tip radius r_T, tip blade angle β_T, and constant pitch:

$$P = 2\pi\, r_T\, \tan\beta_T = 2\pi\, r^*\, \tan\beta$$

The flow is fully wetted everywhere except on the suction

sides of the blades, where attached cavitation occurs. The mean flow velocity $\overline{\boldsymbol{u}}$ in the blade channels is specified by the flow coefficient $\phi = \overline{w}/\Omega\, r_T$, assuming fully-guided forced-vortex flow with zero radial velocity $\overline{u}$, uniform axial velocity $\overline{w}$, and angular velocity $\Omega_F = \overline{v}/r = \Omega/(1 - \phi \cot \beta_T)$. With reference to Figure 2, cavitation is thought to occur on the suction sides of the blades in the form of slowly-moving attached pockets uniformly distributed in a thin layer of given thickness $\delta \ll P$ and damped acoustic admittance $\rho_C\, a_C^2\, (1 + \imath\zeta)$, where ζ is the nondimensional damping coefficient. The static pressure p_C in the cavitating layer is taken equal to the total pressure p_t of the surrounding liquid, assuming that the flow slows down without losses in the low velocity region between the cavities. We define stationary cylindrical coordinates r, ϑ, z with center in O on the axis of the stator, rotating cylindrical coordinates r', ϑ', z' spinning at the rotor speed with center in the same point O, and rotating and whirling cylindrical coordinates r^*, ϑ^*, z^* fixed in the inducer and with center in O^* on its geometric axis, as shown in Figure 3. Then the equations of the blade surfaces are:

$$b = \vartheta^* + \frac{2\pi}{P}\, z^* - \theta_j = 0$$

where $\vartheta_j = 2\pi(j-1)/N_B$ is the angular location of the j-th blade for $j = 1, 2, \ldots, N_B$. The flow velocities in the stationary and rotating frames are related by $\boldsymbol{u} = \boldsymbol{u}' + \boldsymbol{\Omega} \times \boldsymbol{r}$ and, to

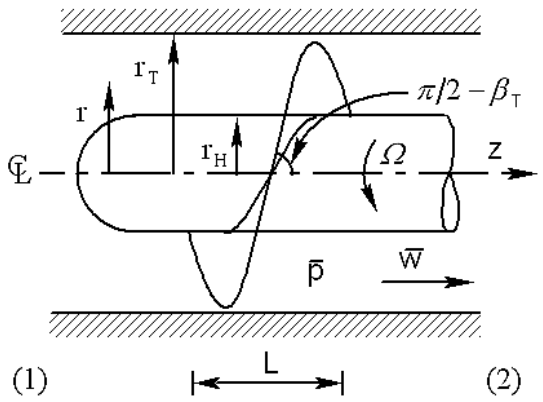

Figure 1: Schematic of the flow configuration and inducer geometry.

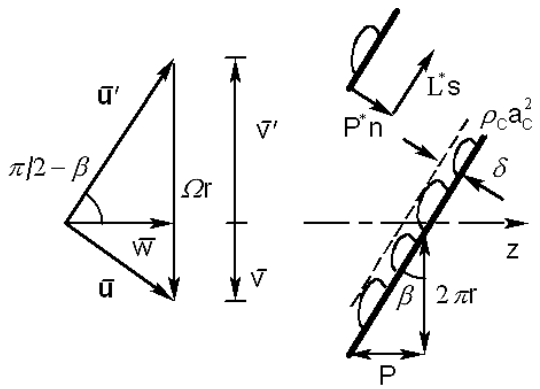

Figure 2: Schematic of the thin layer of attached cavitation pockets on the suction sides of the inducer blades.

the first order in the eccentricity:

$$r^* = r - \varepsilon\, \cos(\vartheta - \omega\, t) = r' - \varepsilon\, \cos(\vartheta' - \omega'\, t)$$
$$\vartheta^* = \vartheta - \Omega\, t + \frac{\varepsilon}{r}\, \sin(\vartheta - \omega\, t) = \vartheta' + \frac{\varepsilon}{r} \sin(\vartheta' - \omega'\, t)$$
$$z^* = z = z'$$

where $\omega' = \omega - \Omega$.

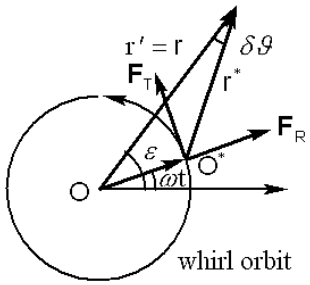

Figure 3: Schematic of whirl motion, coordinates and rotordynamic forces.

Neglecting Coriolis forces, the perturbation velocity $\tilde{\boldsymbol{u}}$ in the frame moving with the mean flow at axial velocity $\overline{w}$ and angular speed Ω_F is irrotational ($\tilde{\boldsymbol{u}} = \nabla\varphi$) because it originates from a resting flow with conservative centrifugal forces. Therefore, in the rotating frame the flow velocity is $\boldsymbol{u}' = (\boldsymbol{\Omega}_F - \boldsymbol{\Omega}) \times \boldsymbol{r} + \overline{\boldsymbol{w}} + \nabla\varphi$ and the Bernoulli's equation writes:

$$\int \frac{\partial' \boldsymbol{u}'}{\partial t} \cdot d\boldsymbol{x} + \frac{1}{2}\boldsymbol{u}' \cdot \boldsymbol{u}' - \frac{1}{2}\Omega^2\, \boldsymbol{r} \cdot \boldsymbol{r} + \frac{p}{\rho_L} = \\ = \int \boldsymbol{u}' \times (\nabla \times \boldsymbol{u}') \cdot d\boldsymbol{x}$$

where $\nabla \times \boldsymbol{u}' = 2\,(\boldsymbol{\Omega}_F - \boldsymbol{\Omega})$. Evaluating this equation between the generic point and the corresponding unperturbed conditions on a vorticity line $r, \vartheta \equiv$ constant, the linearized governing equations for the flow perturbations (tildes) in the rotating frame are:

$$\nabla^2 \tilde{\varphi} = 0 \quad \text{and} \quad \frac{\partial' \tilde{\varphi}}{\partial t} + \overline{\boldsymbol{u}}' \cdot \nabla\tilde{\varphi} + \frac{\tilde{p}}{\rho_L} = 0$$

These equations must be complemented with the appropriate boundary conditions. Here, the flow velocity must satisfy the kinematic conditions $Db/Dt = 0$ on the hub, blade and casing surfaces of equations $b = 0$ in the relevant coordinates. In addition, the total pressure is assumed constant on the inlet and outlet sections of the inducer.

In order to simplify the boundary conditions, let us introduce orthogonal helical coordinates r, n, s of unit vectors $\boldsymbol{e}_r, \boldsymbol{e}_n, \boldsymbol{e}_s$ as shown in Figure 4 with:

$$n = (\vartheta - \vartheta_j)\, \frac{N_B}{2\pi} + z\frac{N_B}{P}$$
$$s = z\frac{\sin^2\beta}{P} - (\vartheta - \vartheta_j)\frac{\cos^2\beta}{2\pi}$$

Here, for convenience, n is normalized with the channel width $P^* = (P/N_B)\cos\beta$ and s with the blade length $L^* = P/\sin\beta$ at the radius corresponding to the angle β. The rotating and body-fixed orthogonal helical coordinates r', n', s'

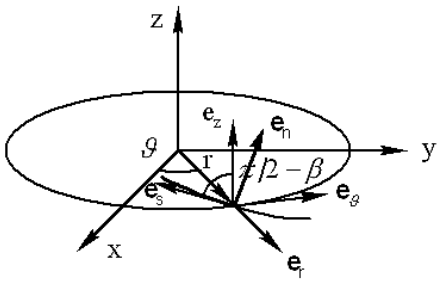

Figure 4: Schematic of the transformation from cylindrical coordinates r, ϑ, z to the orthogonal helical coordinates r, n, s.

and r^*, n^*, s^* are similarly defined in terms of r', ϑ', z' and r^*, ϑ^*, z^*. Then, the equations of the hub, blade pressure sides, blade suction sides and casing surfaces are:

$$b = r^* - r_H = 0$$
$$b = n^* = 0$$
$$b = n^* - 1 + \delta/P^* = 0$$
$$b = r - r_T = 0$$

where $\delta = \delta(t)$. From the continuity equation for the layer $\rho_C \delta \equiv$ constant, the definition of $a_C^2 = dp_t/d\rho_C$ and the Bernoulli's equation $\tilde{p}_t/\rho_L = -\partial\varphi/\partial t$ it follows that:

$$\frac{d\delta}{dt} = \frac{\rho_L\,\delta}{\rho_C\,a_C^2}\,\frac{\partial^2\tilde{\varphi}}{\partial t^2}$$

With these results, expressing $\nabla^2\varphi = 0$ and $\partial b/\partial t + \boldsymbol{u}'\cdot\nabla b = 0$ in the rotating helical coordinates r', n', s':

$$\frac{\partial^2\tilde{\varphi}}{\partial r'^2} + \frac{1}{r'}\,\frac{\partial\tilde{\varphi}}{\partial r'} + \frac{N_B^2}{P^2\cos^2\beta}\,\frac{\partial^2\tilde{\varphi}}{\partial n'^2} + \frac{\cos^2\beta}{4\pi^2 r'^2}\,\frac{\partial^2\tilde{\varphi}}{\partial s'^2} = 0$$

and the linearized boundary conditions are found to be:

$$\frac{\partial\tilde{\varphi}}{\partial r'} = 0 \quad \text{on} \quad r' = r_T$$
$$\frac{\partial\tilde{\varphi}}{\partial r'} = \varepsilon\,(\omega - \Omega_F)\sin H \quad \text{on} \quad r' = r_H$$
$$\frac{\partial\tilde{\varphi}}{\partial n'} = \frac{\varepsilon\,(\omega-\Omega_F)\,P^2\cos^2\beta}{2\pi\,r'\,N_B}\cos H \quad \text{on} \quad n' = 0$$
$$\frac{\partial\tilde{\varphi}}{\partial n'} + K_C\,\frac{\partial^2\tilde{\varphi}}{\partial t^2} = \frac{\varepsilon(\omega-\Omega_F)\,P^2\cos^2\beta}{2\pi\,r'\,N_B}\cos H \quad \text{on} \quad n' = 1$$
$$\frac{\partial\tilde{\varphi}}{\partial t} = 0 \quad \text{on} \quad s' = s'_1 = -\frac{\cos^2\beta}{2N_B},\ s'_1 + N_R$$

where

$$H = \frac{2\pi}{N_B}n'\sin^2\beta - 2\pi\,s' + \vartheta_j - \omega'\,t$$
$$K_C = \frac{\rho_L\,\delta\,P^*}{\rho_C\,a_C^2(1+\imath\zeta)}$$

is a parameter describing the behavior of the cavitating layer, and N_R is the number of revolutions of the blade channels about the inducer axis.

With the above boundary conditions the Laplace equation for $\tilde{\varphi} = \mathsf{Re}\{\hat{\varphi}\}$ yields a well-posed boundary value problem for the complex velocity potential $\hat{\varphi}$. If the variable blade angle β is approximated by a constant value β_M at some suitable mean radius r_M, the separable solution (Lebedev, 1965) in the blade channels $0 \le n' \le 1$ is:

$$\hat{\varphi} = \hat{\varphi}_H + \hat{\varphi}_B$$

where

$$\hat{\varphi}_H = \sum_{k=1}^{+\infty}\sum_{m=1}^{+\infty} R_{km}(r')\,N_k(n')\,S_m(s')\,e^{-\imath\,\omega' t}$$
$$\hat{\varphi}_B = \sum_{l=1}^{+\infty}\sum_{m=1}^{+\infty} R_{lm}(r')\,N_{lm}(n')\,S_m(s')\,e^{-\imath\,\omega' t}$$

are the solutions corresponding to the hub and blade excitation. In the expression of $\hat{\varphi}_H$:

$$R_{km}(r') = I_{km}\,\times$$
$$\times\,\frac{K'_{q_m}(\lambda_k^*\,r_T)\,I_{q_m}(\lambda_k^*\,r') - I'_{q_m}(\lambda_k^*\,r_T)\,K_{q_m}(\lambda_k^*\,r')}{I'_{q_m}(\lambda_k^*\,r_H)\,K'_{q_m}(\lambda_k^*\,r_T) - K'_{q_m}(\lambda_k^*\,r_H)\,I'_{q_m}(\lambda_k^*\,r_T)}$$

$$N_k(n') = \cos\left(n'\sqrt{-\nu_k^2}\right)$$

are the coupled modal solutions corresponding to the hub excitation, where:

$$\lambda_k^* = \frac{N_B}{P\,\cos\beta_M}\sqrt{-\nu_k^2}$$

and $\sqrt{-\nu_k^2}$ are the (complex) principal roots of the equation:

$$\sqrt{-\nu_k^2}\,\sin\sqrt{-\nu_k^2} = -K_C\,\omega'^2\cos\sqrt{-\nu_k^2}$$

Similarly, in the expression of $\hat{\varphi}_B$:

$$R_{lm}(r') = Y'_{q_m}(\lambda_{lm}r_H)\,J_{q_m}(\lambda_{lm}r') - J'_{q_m}(\lambda_{lm}r_H)\,Y_{q_m}(\lambda_{lm}r')$$

$$N_{lm}(n') = \frac{I(1)\cosh(\nu_{lm}\,n') - I(0)\cosh[\nu_{lm}(n'-1)]}{\nu_{lm}\sinh\nu_{lm} - K_C\,\omega'^2\cosh\nu_{lm}} +$$
$$-\,\frac{I(0)\,K_C\omega'^2}{\nu_{lm}\sinh\nu_{lm} - K_C\,\omega'^2\cosh\nu_{lm}}\,\frac{\sinh[\nu_{lm}(n'-1)]}{\nu_{lm}}$$

are the coupled modal solutions corresponding to the blade excitation, where λ_{lm} are the (positive) roots of the equation:

$$J'_{qm}(\lambda\,r_H)\,Y'_{q_m}(\lambda\,r_T) - Y'_{q_m}(\lambda\,r_H)\,J'_{q_m}(\lambda\,r_T) = 0$$
$$\nu_{lm} = \lambda_{lm}\frac{P\cos\beta_M}{N_B}$$

and

$$I(n') = \frac{\varepsilon(\omega-\Omega_F)P^2\cos^2\beta_M}{\pi N_B N_R}e^{\imath[(2\pi/N_B)n'\sin^2\beta_M+\vartheta_j]}\,\times$$
$$\times\,\frac{\int_{r_H}^{r_T}R_{lm}(r')\,dr'}{\int_{r_H}^{r_T}R_{lm}^2(r')\,r'\,dr'}\int_{s'_1}^{s'_1+N_R}e^{-\imath 2\pi\,s'}\,S_m(s')\,ds'$$

Finally, in both of the expressions of $\hat{\varphi}_H$ and $\hat{\varphi}_B$:

$$q_m = \frac{m}{2N_R}\cos\beta_M \quad \text{and} \quad S_m(s') = \sin\frac{m\pi(s'-s'_1)}{N_R}$$

The instantaneous fluid force on the inducer is:

$$\tilde{\boldsymbol{F}} = \oint_{S_H \cup S_B} p(\, x'|_{\varepsilon \neq 0}\,, t)\, d\boldsymbol{S}$$

where the pressure:

$$p = \overline{p} - \rho_L \left(\frac{\partial \tilde{\varphi}}{\partial t} - \frac{\Omega_F - \Omega}{2\pi} \frac{\partial \tilde{\varphi}}{\partial s'} \right)$$

is evaluated for $\varepsilon \neq 0$ at the perturbed position of the hub and blade surfaces S_H and S_B. Thus, expanding to the first order in the eccentricity and noting that the mean pressure $p(r'|_{\varepsilon=0}\,, t)$ makes no net contribution to the force on the inducer in its centered position, the following equation is obtained:

$$\tilde{\boldsymbol{F}} \approx - \oint_{S_H \cup S_B} \left[\left. \frac{\partial \overline{p}}{\partial r'} \right|_{\varepsilon=0} \left(r'|_{\varepsilon \neq 0} - r'|_{\varepsilon=0} \right) + \tilde{p}(\boldsymbol{x}'|_{\varepsilon=0}\,, t) \right] d\boldsymbol{S}$$

Here the first term is the buoyancy force on the displaced inducer due to the radial gradient of the mean pressure:

$$\frac{d\overline{p}}{dr'} = \rho_L \Omega^2 r' \left(1 - \phi^2 \cot^2 \beta_T\right)$$

and the second term is the force due to the pressure perturbations generated by the eccentric motion. The components of the instantaneous rotordynamic force are therefore obtained by integrating the projections of the elementary pressure forces along the axes of the whirling frame of center in O^* and unit vectors $\boldsymbol{e}_R, \boldsymbol{e}_T, \boldsymbol{e}_z$, as shown in Figure 5. Finally, further integration over a period $2\pi/\omega'$ yields the time-averaged rotordynamic force $\overline{\boldsymbol{F}}$ on the inducer.

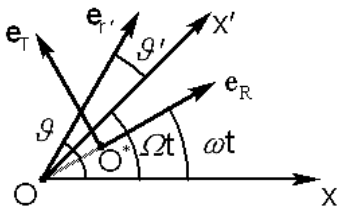

Figure 5: Schematic of the transformation from the rotating frame $O, \boldsymbol{e}_{r'}, \boldsymbol{e}_{\vartheta'}, \boldsymbol{e}_{z'}$ to the whirling frame $O^*, \boldsymbol{e}_R, \boldsymbol{e}_T, \boldsymbol{e}_z$

The entire flow has therefore been determined in terms of the material properties of the two phases, the geometry of the inducer, the nature of the excitation, and the assigned quantities ϕ, δ, ρ_C, a_C and ζ.

RESULTS AND DISCUSSION

The rotordynamic fluid forces predicted by the present model are compared with the data measured by Bhattacharyya (1994) on a three-bladed helical inducer with $r_T = 5.06$ cm, $r_H/r_T = 0.4$, $\beta_T = 9^o$, $L = 2.43$ cm, $\varepsilon = 0.254$ mm. The data refer to operation in water at room temperature, rotational speed $\Omega = 3,000$ rpm, variable whirl speed, and several values of the inlet flow coefficient $\phi_1 = \dot{Q}/A_1 \Omega r_T$ (not corrected for hub blockage) and cavitation number $\sigma_1 = (p_1 - p_V)/\frac{1}{2}\rho_L \Omega^2 r_T^2$.

Figure 6 shows some typical experimental results for the nondimensional rotordynamic force $\tilde{\boldsymbol{f}} = \overline{\boldsymbol{F}}/\pi\varepsilon^2 P \rho_L \Omega^2\, r_T$ on the sample inducer tested under developed cavitation at $\phi_1 = 0.049$ and $\sigma_1 = 0.106$. Notice that the radial and tangential force components do not vary quadratically with the normalized whirl speed ω/Ω, and that their behavior is characterized by multiple zero crossings. The radial force (Figure 6a) is essentially positive (destabilizing) for $\omega/\Omega < -0.2$, oscillates above and below zero for $-0.2 < \omega/\Omega < 0.3$, and remains essentially negative (stabilizing) for $\omega/\Omega > 0.3$. Similar behavior was observed for other cavitation numbers (Bhattacharyya, 1994). The tangential force (Figure 6b) is positive over most of the sampled frequencies, but also exhibits rapid oscillations near the origin. In all of the experiments of Bhattacharyya a peculiar feature of the tangential force is the occurrence of a sharp positive (destabilizing) peak at $\omega/\Omega \approx 0.2$, whose intensity increases at higher cavitation numbers and lower flow coefficients.

Figure 6 also shows the rotordynamic forces predicted by the present model (continuous line) assuming $\mathrm{Re}\left\{K_C \Omega^2\right\} = 2.5$ for the real part of the cavitation parameter and $\zeta = 0.045$ for

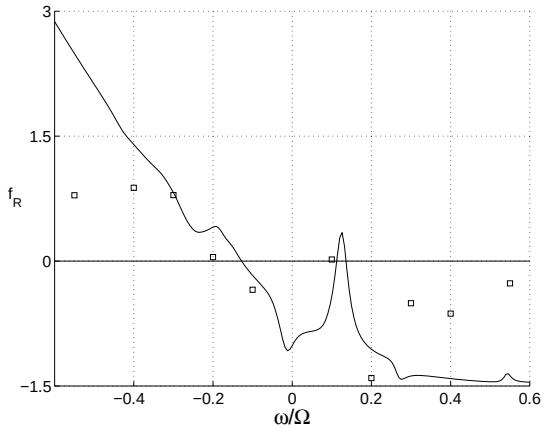

(a) Radial rotordynamic force

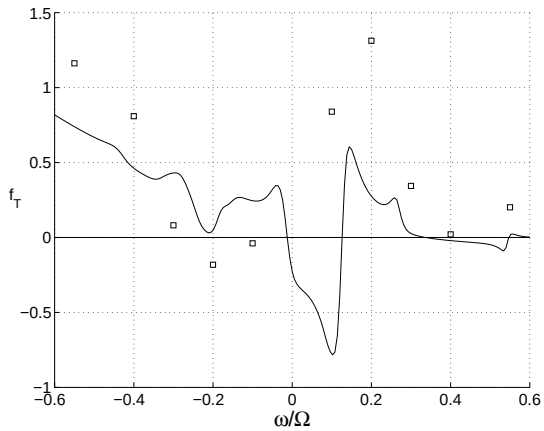

(b) Tangential rotordynamic force

Figure 6: Nondimensional rotordynamic forces f_R and f_T on the test inducer as a function of the ratio ω/Ω of the whirl and rotational speeds. The experimental values (circles) obtained by Bhattacharyya (1994), under developed cavitation conditions at $\phi_1 = 0.049$ and $\sigma_1 = 0.106$ are compared with the model predictions (solid line) for $\phi = \phi_1/(1 - r_H^2/r_T^2) = 0.0583$, $\mathrm{Re}\left\{K_C\, \Omega^2\right\} = 2.5$, $\zeta = 0.045$ and $N_R = 0.285$.

the nondimensional damping coefficient. An effective value of the nondimensional blade channel length, $N_R = 0.285$, intermediate between the geometric length of the blades and their actual overlap, has been used in the computations in order to empirically compensate for the errors introduced by the formulation in orthogonal helical coordinates. In addition, the pressure gradient of the mean flow has been evaluated for a decreased value of the swirl speed Ω_F in order to account for the gradual rotational acceleration of the flow entering the inducer. Comparison with the experimental data shows that, in spite of its approximate nature, the present theory correctly captures the observed magnitude of the rotordynamic forces and the salient features of their whirl frequency spectrum, including their stabilizing or destabilizing effects on the eccentric motion of the inducer.

The complex dependence of the lateral rotordynamic fluid forces on the whirl speed is due to the occurrence of internal resonances of the cavitating flow in the blade channels under the excitation generated by the whirl motion of the inducer. Given the functional dependence of the solution, it appears that the system has an infinite set of (generally complex) critical whirl speeds:

$$\omega'_{lm} = \omega_{lm} - \Omega = \pm\sqrt{\frac{\nu_{lm}\tanh\nu_{lm}}{K_C}}$$

symmetrically located above and below the rotational speed Ω (synchronous conditions). The critical speeds are seen to depend on the mode numbers of the flow perturbations and the parameter K_C used to characterize the occurrence of cavitation on the suction sides of the blades. The extent of cavitation increases when the value of this parameter is varied from zero, corresponding to fully-wetted flow conditions, to larger and larger values. In the special case of no cavitation damping ($\zeta = 0$), K_C is real and the boundary value problem for $\hat{\varphi}$ is self-adjoint, with real eigenvalues λ^2 and ν^2. In the presence of damping, the series for $\hat{\varphi}$ converge rapidly even for low subcritical values of $\zeta \ll 1$, and only the first few modes are needed in the computations. For these modes the eigenvalues are of order unity or slightly larger. Since cavitating flows are inherently dissipative, it follows that the critical whirl speeds of practical importance tend to concentrate in two small ranges just above and below synchronous conditions as soon as the intensity of cavitation is sufficient for raising the real part of $K_C\Omega^2$ well above unity.

The relation of K_C to the extent of cavitation can be investigated with the help of a suitable flow model. Here we make use of the classical quasi-homogeneous isenthalpic cavitation model with thermal effects described by Brennen (1995) and modified by Rapposelli and d'Agostino (2001) to account for the concentration of active nuclei. The behavior of the real part of $K_C\Omega^2$ with the local void fraction α is illustrated in Figure 7 for water at room and boiling temperature. The results depend parametrically on the blade channel blockage δ/P^* and the ratio δ_T/R between the thermal boundary layer thickness surrounding a spherical cavity and the radius of the cavity itself. The parameter δ_T/R is nearly constant during the thermally controlled growth of cavitating bubbles and its value can be estimated as a function of the flow conditions, the thermophysical properties of the two phases, and the concentration of active cavitation nuclei (Rapposelli and d'Agostino, 2001). Here the choice of a higher blockage δ/P^* at the boiling temperature reflects the greater penetration of cavitation in the liquid at elevated temperatures. From Figure 7 it appears that the value $\mathrm{Re}\left\{K_C\Omega^2\right\}$ previously used for the prediction of the rotordynamic forces would correspond to void fractions ranging from 4×10^{-2} at room temperature to 10^{-1} at boiling conditions. The average separation between bubbles would then be on the order of 2 to 3 diameters, not unrealistic mean values for typical cavitation on inducer blades.

The influence of the cavitation parameter on the solution is illustrated by the waterfall plots of Figure 8. The figure clearly show that the degree of cavitation has a major impact in locating the critical speeds and determining the magnitude of the rotordynamic forces as functions of the whirl speed. Two sets of subsynchronous and supersynchronous resonances are predicted. At higher values of the cavitation parameter the amplitudes of the resonances decrease, as their frequencies approach synchronous conditions. At low values of $\mathrm{Re}\left\{K_C\Omega^2\right\}$ the void fraction is likely to violate the condition:

$$(\alpha\,\delta)_{min} \approx \varepsilon\,\sin\beta_M$$

for the survival of the cavitating layer during a complete oscillation cycle of the whirl motion. With typical choices of the relevant quantities, the minimum void fraction is estimated to be $\alpha_{min} \approx 10^{-2} \div 10^{-1}$. Hence, using the results of Figure 7, the physically significant solutions of the present theory are restricted to minimum values of the cavitation parameter:

$$\mathrm{Re}\left\{K_C\,\Omega^2\right\}_{min} \approx 1 \text{ to } 10$$

respectively corresponding to room temperature and boiling conditions. In this range Figure 8 indicate the presence of two relatively weak subsynchronous critical speeds near $\omega/\Omega \approx 0.5$, and a second couple of considerably more intense supersynchronous critical speeds in the vicinity of $\omega/\Omega \approx 1.5$. The spectral locations of these critical speeds evocatively overlap with the reported ranges of free-whirl instabilities in cavitating turbopumps.

As a final comment, comparison of the data reported in Figure 6 with the results of Figure 8 indicates that the scant experimental information currently available on the behavior of

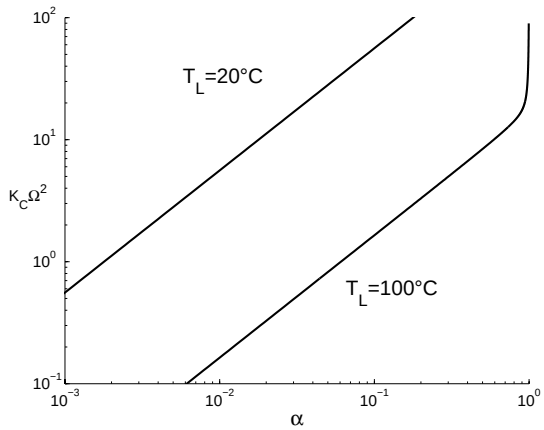

Figure 7: Nondimensional cavitation parameter $K_C\,\Omega^2$ as a function of the void fraction in the cavitating layer for undamped operation in water at $T_L = 20^oC$ ($\delta_T/R = 0.3$, $\delta/P^* = 3\%$) and $T_L = 100^oC$ ($\delta_T/R = 1$, $\delta/P^* = 10\%$).

rotordynamic forces in cavitating turbopumps only covers a limited portion of the frequency spectrum, and probably not the most significant one in connection with the onset of cavitation-induced whirl instabilities.

LIMITATIONS

We now briefly examine the restrictions imposed to the present theory by the various simplifying approximations that have been made. Specifically we shall discuss the limitations due to the assumption of thin-layer cavitation, to the neglect of Coriolis forces, to the applicability of the formulation in orthogonal helical coordinates to the analysis of cavitating inducers, and to the use of the linear perturbation approach in deriving the solution.

The assumption of thin-layer cavitation implies that the thickness of the cavitating region is significant smaller than the blade channel width and that its properties can be approximated as constant over the entire length of the blades for the purpose of evaluating the rotordynamic forces. Although clearly none of these conditions is rigorously met in cavitating inducers, comparison with earlier results obtained by d'Agostino and his collaborators (1997,1998) for uniformly distributed bubbly cavitation shows that the predicted values of the rotordynamic forces are remarkably independent on the precise geometry of flow cavitation.

The neglect of Coriolis forces implies that $\Omega_F \ll \Omega$, a condition that is approximately satisfied in lightly loaded inducers.

For the formulation in orthogonal helical coordinates to be valid the geometric length of the blades should be comparable to their actual overlap, which is rarely the case in low blade angle inducers. Formally, this is probably one of the most stringent limitations of the present analysis and can only be partially circumvented by artificially introducing an empirical "effective length" of the blade channels.

Finally, the perturbation approach simply requires that $\varepsilon \ll r_T$, a condition that can safely be assumed in the analysis of whirl instabilities of cavitating turbomachines.

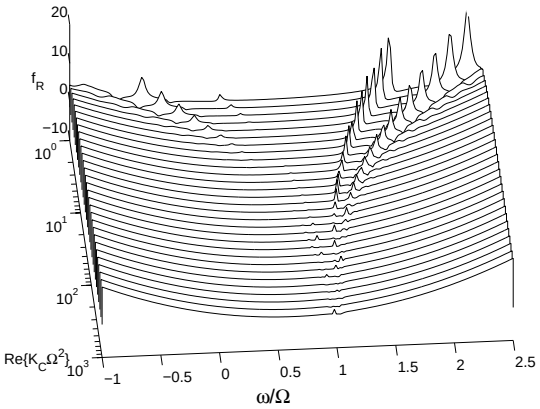

(a) Radial rotordynamic force

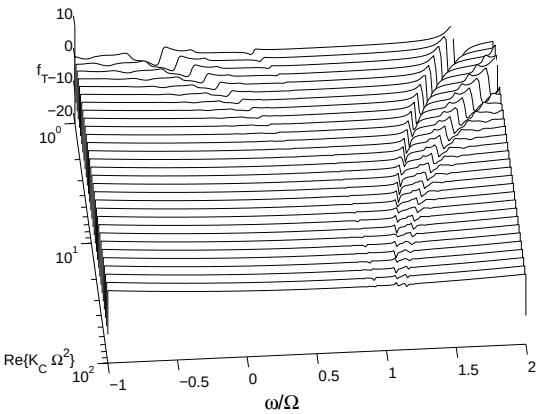

(b) Tangential rotordynamic force

Figure 8: Waterfall plots of the nondimensional rotordynamic forces f_R and f_T on the test inducer as a function of the ratio ω/Ω of the whirl and rotational speeds and the real part of the nondimensional cavitation parameter, $K_C\,\Omega^2$. The flow coefficient is $\phi = 0.0583$, the nondimensional damping coefficient is $\zeta = 0.045$ and the effective length of the blade channels is $N_R = 0.285$.

SUMMARY AND CONCLUSIONS

This investigation reveals a number of important flow phenomena occurring in whirling and cavitating helical inducers. The results clearly indicate that blade cavitation drastically modifies the rotordynamic forces exerted on the impeller by the surrounding fluid. The dynamic response of the cavitating flow to the periodic excitation imposed by the whirl motion generates multiple subsynchronous and supersynchronous flow resonances in the blade channels, interfering with the more regular spectral behavior of the rotordynamic fluid forces, typical of noncavitating operation. The extent of cavitation has a major impact in locating the critical speeds and determining the intensity of flow-induced rotordynamic forces. At higher levels of cavitation the amplitudes of the flow resonances decrease, and their frequencies approach the rotational speed of the impeller (synchronous conditions). In spite of its approximate nature, the present theory correctly captures the main observed features of the rotordynamic forces. More generally, we are confident that it contributes some useful fundamental insight into the complex physical phenomena responsible for the onset and sustain of free-whirl instabilities in cavitating turbopumps.

ACKNOWLEDGEMENTS

The present work has been partially supported by the Agenzia Spaziale Italiana under a 1999 grant for fundamental research. The authors would like to acknowledge the help of Mr. Emilio Rapposelli in the implementation of the isenthalpic cavitation model, and express their gratitude to Prof. Mariano Andrenucci, Director of Centrospazio, Ospedaletto (Pisa), Italy, and to Prof. Renzo Lazzeretti of the Dipartimento di Ingegneria Aerospaziale, Università di Pisa, Pisa, Italy, for their constant and friendly encouragement.

REFERENCES

Adkins, D. R. and Brennen, C. E., 1988. "Analysis of Hydrodynamic Radial Forces on Centrifugal Pump Impeller." *ASME Journal of Fluids Engineering*, vol. 110, pp. 20–28.

Arndt, N. and Franz, R., 1986. Observations of Hydrodynamic Forces on Several Inducers Including the SSME LPOTP. Ph.D. thesis, Division of Engineering and Applied Sciences, California Institute of Technology, Pasadena, California. Report No. E249.3.

Baskharone, E. A., 1999. "Swirl Brake Effect on the Rotordynamic Stability of a Shrouded Impeller." *ASME Journal of Turbomachinery*, vol. 121, pp. 127–133.

Bhattacharyya, A., 1994. Internal Flows and Force Matrices in Axial Flow Inducers. Ph.D. thesis, California Institute of Technology.

Brennen, C. E., 1994. Hydrodynamics of Pumps. Concepts ETI, Inc. and Oxford University Press, Concepts ETI, Inc. P. O. Box 643, Norwich, Vermont 05055, USA — Oxford University Press, Walton Street, Oxford OX2 6DP, England. ISBN 0-933283-07-5 (Concepts ETI, Inc.), 0-19-856442-2 (Oxford University Press).

Brennen, C. E., 1995. Cavitation and Bubble Dynamics. Oxford Engineering Science Series. Oxford University Press, New York. ISBN 0-19-509409-3.

Chamieh, D. S., Acosta, A. J., Brennen, C. E., and Caughey, T. K., 1985. "Experimental Measurements of Hydrodynamic Radial Forces and Stiffness Matrices for a Centrifugal Pump Impeller." *ASME Journal of Fluids Engineering*, vol. 107, pp. 307–315.

d'Agostino, L. and d'Auria, F., 1997. "Three-Dimensional Analysis of Rotordynamic Forces on Whirling and Cavitating Inducers." In "ASME Fluids Engineering Division Summer Meeting, June 22–26," vol. ASME Paper FEDSM97-3335. Vancouver, British Columbia, Canada.

d'Agostino, L., d'Auria, F., and Brennen, C. E., 1998. "A Three-Dimensional Analysis of Rotordynamic Forces on Whirling and Cavitating Helical Inducers." *ASME Journal of Fluids Engineering*, vol. 120, pp. 698–704.

d'Auria, F., d'Agostino, L., and Brennen, C. E., 1995. "Bubble Dynamics Effects on the Rotordynamic Forces in Cavitating Inducers." In "ASME Cavitation and Multiphase Flow Forum," vol. FED 201. Hilton Head Island, South Carolina.

Jery, B., 1987. Experimental Study of Unsteady Hydrodynamic Force Matrices on Whirling Centrifugal Pump Impellers. Ph.D. thesis, Division of Engineering and Applied Sciences, California Institute of Technology, Pasadena, California. Report No. E200.22.

Jery, B., Acosta, A. J., and Caughey, T. K., 1985. "Forces on Centrifugal Pump Impellers." In "Proceedings of 2nd International Pump Symposium, Texas, April 29 – May 2," Houston, Texas, USA, pp. 21–32.

Lebedev, N. N., 1965. Special Functions and Their Applications. Prentice Hall.

Ohasi, H. and Shoji, H., 1987. "Lateral Fluid Forces on Whirling Centrifugal Impeller (2nd Report: Experiment in Vaneless Diffuser)." *ASME Journal of Fluids Engineering*, vol. 109, pp. 100–106.

Rapposelli, E. and d'Agostino, L., 2001. "A Modified Isenthalpic Model of Cavitation in Plane Journal Bearings." In "Proceedings of Fourth International Symposium on Cavitation," vol. CAV2001:Session B5.003. Pasadena, California.

Rosenmann, W., 1965. "Experimental Investigations of Hydrodinamically Induced Shaft Forces with a Three Bladed Inducer." In "Proc. ASME Symp. on Cavitation in Fluid Machinery," .

Shoji, H. and Ohasi, H., 1987. "Lateral Fluid Forces on Whirling Centrifugal Impeller (1st Report: Theory)." *ASME Journal of Fluids Engineering*, vol. 109, pp. 94–99.

Tsujimoto, Y., Yoshida, Y., Ohashi, H., Teramoto, N., and Ishizaki, S., 1997. "Fluid Force Moment on a Centrifugal Impeller Shroud in Precessing Motion." *ASME Journal of Fluids Engineering*, vol. 119, pp. 366–371.

Uy, R. V. and Brennen, C. E., 1999. "Experimental Measurments of Rotordynamic Forces Caused by Front Shroud Pump Leakage." *ASME Journal of Fluids Engineering*, vol. 121, pp. 633–637.